ACS OMEGA

http://pubs.acs.org/journal/acsodf

Article

Inhibition of Methane Hydrates Using Biodegradable Additives

Burla Sai Kiran and Pinnelli S. R. Prasad*

Cite This: *ACS Omega* 2021, 6, 8261−8270

Read Online

ACCESS | Metrics & More | Article Recommendations

ABSTRACT: Prevention of hydrate plugs during transportation of oil and natural gas in the pipeline network is challenging. Certain additives are often introduced into the process to eliminate/delay plug formation. Dominantly synthetic inhibitors are deployed in large volumes (~20 to 30% by volume) to counter the problem and are highly expensive and, in some circumstances, toxic. The search for novel additives that are eco-friendly and act as inhibitors is in demand. The present study reports the thermodynamic inhibition (THI) capacity of some vastly available natural biopowders, such as *Azadirachta indica* (neem), *Piper betel* (betel), and *Nelumbo nucifera* (Indian lotus) in low dosage (0.5 wt %), on methane hydrate (MH) formation. Since the gas flow is dynamic, experiments are conducted in stirred geometry by varying the speed range from 0 to 1000 rotations per minute (rpm). All of the studies are performed in the isochoric method procedure. The biopowders act as efficient thermodynamic hydrate inhibitors. Once the nucleation triggers, they act as kinetic hydrate promoters. Since sodium dodecyl sulfate (SDS) is an excellent kinetic hydrate promoter in both stirred and nonstirred geometries, the obtained results are compared with the SDS system. Hydrate nucleation is triggered at higher subcooling (~8 to 10 K) in the presence of water-soluble bioextracts. The neem leaf extracts showed a ~30% lower hydrate conversion than SDS in identical experimental conditions. Two-stage hydrate nucleation occurred at higher stirring speeds, and the hydrate conversion is inferior (~6%) between the primary and secondary stages. The addition of biopowder extracts is useful in controlling hydrate formation. A small quantity of biopowders provides higher inhibition and reduces synthetic chemicals used in real-time applications.

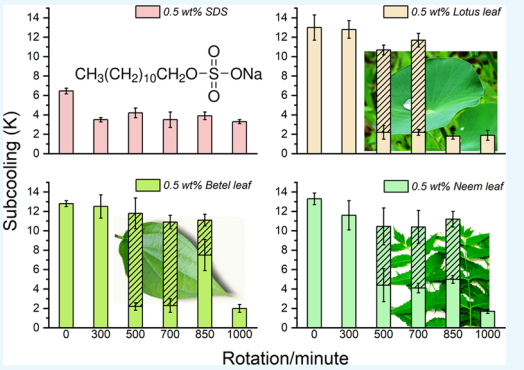

INTRODUCTION

Gas hydrates termed as "clathrates" are crystalline compounds in which gas molecules are captured inside the cages formed by water molecules. Hydrogen bonding develops water cages at suitable pressure and temperature conditions. Gas molecules' motion is confined inside these water cages through week van der Waals interactions. The most common naturally occurring gas hydrates are mainly saturated hydrocarbons (e.g., methane, ethane, propane, butane). Other gases like carbon dioxide, nitrogen, and hydrogen sulfide can form clathrates at suitable temperature and pressure conditions.[1] The volumetric concentration of gas molecules in the hydrate cages is larger by 180 at standard temperature and pressure (STP) conditions.[2] In nature, the gas hydrates are available in deep ocean and permafrost regions.[3] The energy estimated in hydrates is twice comparative to all other forms of hydrocarbon sources.[1] Natural gas hydrates, consisting mostly of methane gas, could serve as a future fuel source.[4,5] Depending upon the nature of the guest molecule, the structures of the hydrates are classified into three types, namely, structure I (sI), structure II (sII), and structure H (sH).[1] Unveiling of hydrates was first proposed by Sir Humphrey Davy in 1810.[1] Later, its importance was signified in 1934 by its debut in blocking pipelines in the hydrocarbon industry.[6] A molecular-level understanding of the hydrates is still obscure and requires further elaborated investigations.

The gas hydrate study got scientific attention due to the blockage of gas pipelines.[6] In the flow assurance sector, the hydrate occurrence in gas flow lines' is a significant issue. The oil and gas companies spend millions of dollars annually to restrict this hydrate occurrence.[7] Obstruction/blockage of these flow lines affects the production and is a significant safety factor; choking may lead to induced explosion. It releases hydrocarbons into the environment, a hazardous havoc.[1,8] Of the three structures, structures I and II are ascertained in oil and gas production and processing.[2] The primary means of natural gas transportation is through pipelines. These pipelines are deployed at the ocean bottom, where the temperature is around 4 °C, and on land, where the temperature is maximum during summers and extremely lower in winters. Methane gas is the principal constituent of natural gas, transported via

Received: December 30, 2020
Accepted: February 25, 2021
Published: March 15, 2021

pipelines. Water and favorable conditions (high pressures and low temperatures) trigger the hydrate occurrence in the pipe column. The hydrate crystal grows enormously across the walls and obstructs the gas flow. Intense research is pursued to overcoming these significant issues.[9,10] Despite gas hydrates being an obstruction in gas flow systems, the hydrate terminology leads to multifaceted applications, like natural gas storage and transportation, carbon sequestration, separation of gases, desalination, and heavy metal separation.[11−15]

The conventional methods adopted to eliminate the plugging formation are removing water; pipeline insulation; depressurizing; and the addition of glycols, alcohols, silica gel, and hygroscopic salts into the pipeline.[16−18] Hydrate inhibition is categorized into two groups: thermodynamic hydrate inhibitors (THIs) and low-dosage hydrate inhibitors (LDHIs). THIs work by altering the hydrate formation conditions to much lower temperatures and high pressures, shifting the phase equilibrium curve distinctly when compared to that of the pure system. To execute the process, the THIs are added in high concentrations (10−60%), which is expensive and, in some circumstances, the toxic nature of these chemicals hamper real-time use. Examples of THIs are methanol, monoethylene glycol, diethylene glycol, tetramethylammonium hydroxide, ethanol, etc.[19−25] In a similar fashion, LDHIs retard the hydrate growth, and they are used in significantly lower concentrations (<2 wt %). The LHDIs are further subdivided into kinetic hydrate inhibitors (KHIs) and antiagglomerates (AA's). The KHIs delay the hydrate onset point and decelerate the hydrate growth rate, where AAs act on surface-active compounds and prevent small hydrate particles' growth into hydrate plugs. These LDHIs do not alter the hydrate equilibrium conditions but retard the gas uptake rate by hindering the crystal growth.[25−28] Examples of KHIs are poly(vinyl caprolactam) (PVCap), *N*-methyl-*N*-vinyl acetamide, poly (*N*-vinylpyrrolidone) (PVP), poly(ethylene oxide) (PEO), etc. Their use is limited as they have high cost and show insufficient biodegradation.[29,30] Ester polymer, butyl sulfate, sodium valerate, tetra-*n*-butyl ammonium bromide, etc. are well-known AAs.[31−37]

In recent times, research on natural biomaterials/additives is pursued rigorously. Xu et al. exposed pectin as a natural hydrate kinetic inhibitor material. Pectin is a type of polysaccharide found in vegetables and ripe fruits. The pectin has a structure that is environmentally friendly and has high degradability. A small dose (0.25 wt %) of pectin inhibits methane hydrate formation and requires a long induction time, which is ten times more than that of the commercial hydrate inhibitor.[38] Tian et al. examined the role of various cyclodextrins in methane hydrate formation. Cyclodextrins are a family of cyclic oligosaccharides produced from starch. Significantly less quantity (ppm) is used for sampling, and the results demonstrate that all of the components inhibited the methane hydrate growth. When used in addition to sodium dodecyl sulfate (SDS), few samples promoted the hydrate growth depending on the complex structure developed due to the concentration and functional group.[39] Sanatgar and Peyvandi demonstrated the role of edible additives, guar gum and Arabic gum, in methane hydrate formation. Guar gum is a galactomannan polysaccharide extracted from guar beans, and Arabic gum is a natural gum exuded from acacia tree. Guar gum with 0.05 wt % concentration delayed hydrate nucleation (high induction time) and reduced the hydrate growth rate (sluggish kinetics).[40] Efiong et al. performed experiments in a mini flow loop experimental setup. Compressed natural gas (CNG) containing 98.44% CH_4 and 1.50% CO_2 is used in the process. The results are compared with 2-(dimethylamino)-ethyl methacrylate (2-DMEM) and *N*-vinyl caprolactam (N-VCap). The locally formulated inhibitor from agrowaste is used in concentrations of 0.01, 0.02, and 0.03 wt %. Results indicate that the locally formulated inhibitor shows a high inhibition effect equal to that of traditional hydrate inhibitors.[41] Elechi et al. also studied the inhibitory effect of bioadditives in a mini hydrate flow loop system, with CNG containing 98.44% CH_4 and 1.50% CO_2. Cactaceae extract, a medicinal plant available across the tropics of Asia, Africa, and America, is used in 1−3 wt % as a sample solution. The bioextracts show higher inhibition efficiency than conventional monoethylene glycol.[42] Tang et al. studied various green inhibitors and concluded that amino acids, antifreeze proteins, and ionic liquids, at lower concentrations, are effective kinetic inhibitors, and ionic liquids at higher concentrations can be used as prominent thermodynamic inhibitors.[43] These additives are environmentally friendly but lack an economic factor. In recent times the use of amino acids is proposed for the methane and carbon dioxide hydrate inhibitions.[43−47] The use of several chemicals would assist in gas hydrate inhibitory effects, but they lack economic and toxic nature. The mere interest is aimed at identifying novel and eco-friendly additives that act as efficient hydrate inhibitors.[38,48,49] On the other hand, we examined some bioadditives and found them useful for LDHI applications.[12]

The objective of the present study is to assess the inhibitory effect of aqueous solutions made from the dry powders of three naturally occurring leaves, *Nelumbo nucifera* (India lotus), *Piper betel* (betel), and *Azadirachta indica* (Neem). These bio powders have the potential constituents to act as thermodynamic hydrate inhibitors. Since these are naturally available in all seasons, biodegradable, and cost-effective, they are suitable to use as THIs for methane hydrates. Promoting the use of biodegradable additives reduces the release of synthetic chemicals into the environment.

EXPERIMENTAL SECTION

Materials. Methane gas (99.95% purity) is used to perform experiments procured from Bhuruka Gas Company. Deionized water type 1 is used to make the sample solution. The sample leaves were dried at ambient temperature for several days, and the dried leaves are powered in a domestic mixer (Philips-HL1643) and were sieved using a BSS-60 sieve. The sample powder 0.5 wt % is added to the required amount of water and stirred for 30 min using a magnetic spinner, and the homogeneous mixed solution is filtered with what man filter paper. The refined and filtered solution is used as a reactant.

Apparatus. The apparatus includes a high-pressure reactor vessel (100 mL volume) made of SS-316, consisting of a stirrer headward to agitate the sample solution and hold up the pressure up to 10 MPa. The temperature control is by a closed-loop chiller (CLASSIC-AL-RCC-90) using glycol and water mixture in the selected ratio as a coolant. The temperature and pressure measurements were measured using a platinum resistance thermometer (Pt100) and a pressure transducer (WIKA, type A-10 for pressure range 0−25 MPa with ±0.5% accuracy). The stirrer rotations are controlled by a motor speed controller, which ranges from 0 to 1300 rpm.

Procedure. The experiments are performed in a batch reactor following the isochoric method procedure. The filtered

https://dx.doi.org/10.1021/acsomega.0c06328
ACS Omega 2021, 6, 8261−8270

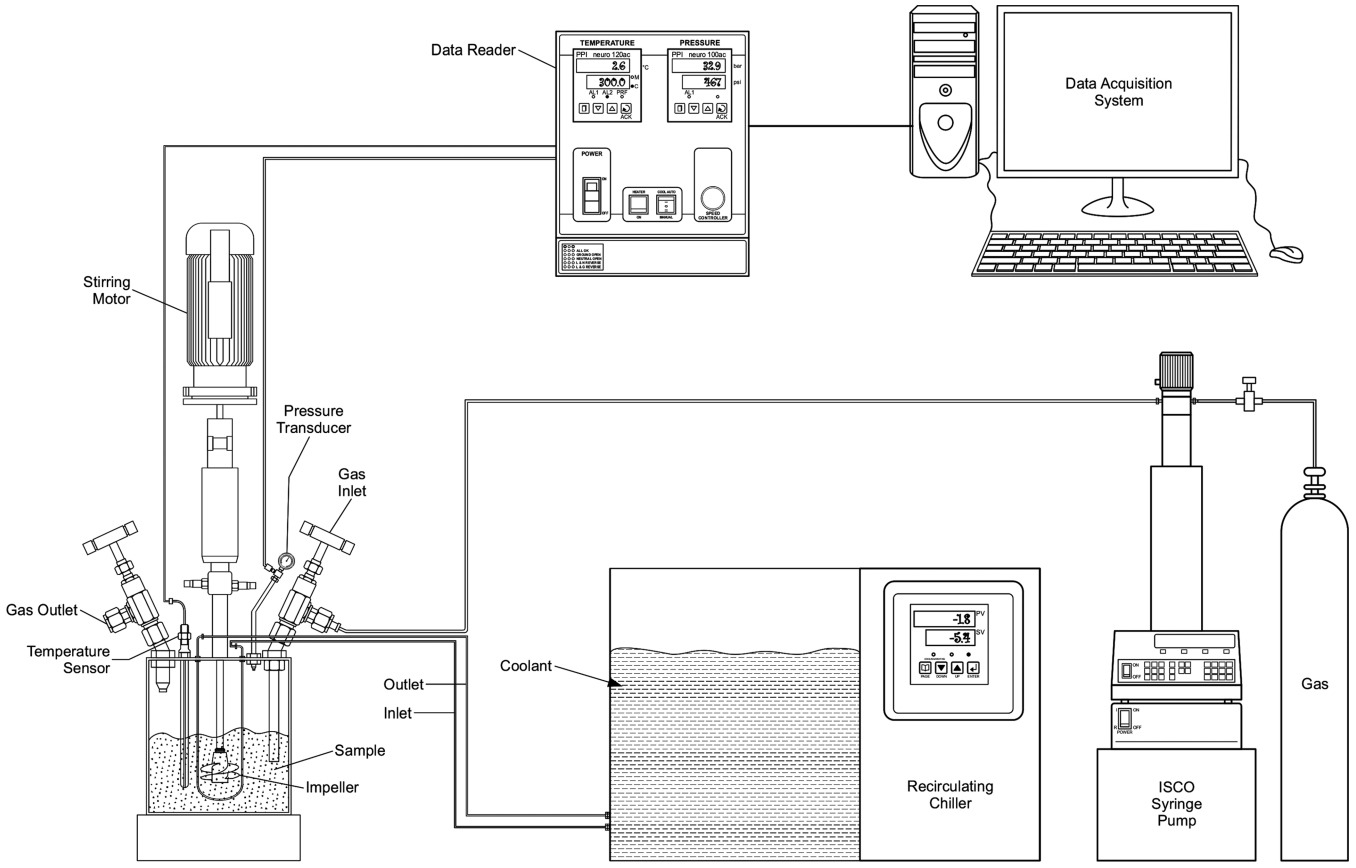

Figure 1. Schematic experimental setup designed to study the process.

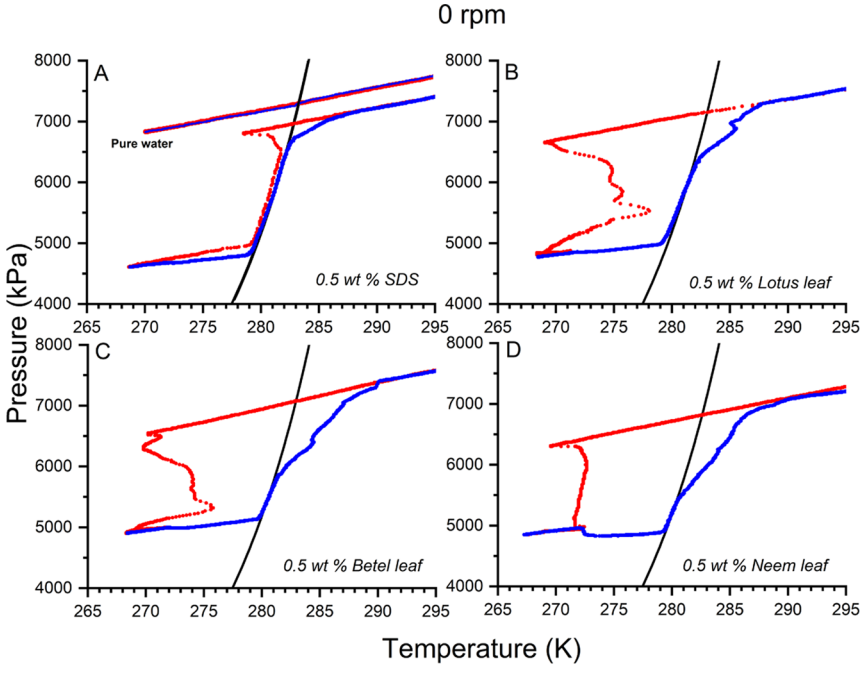

Figure 2. $p-T$ trajectories for the different bio powder extracts performed at 0 rpm. (A) 0.5 wt % SDS, (B) 0.5 wt % lotus leaf, (C) 0.5 wt % betel leaf, and (D) 0.5 wt % neem leaf. In the segment, a cycle performed with pure water is shown in segment A. The red dotted line indicates the cooling cycle, and the blue dotted line indicates the thawing cycle. The black line is the theoretical phase boundary curve for methane hydrate computed from CSM GEM.

aqueous sample solution (29 g) is poured into the reactor vessel. The experiments are performed in dynamic conditions. It is difficult and grueling to framework the pipeline model in the laboratory environment; instead, the tests in the stirred reactor could help understand the MH system's inhibitory effect.[50−52] We conducted MH formation at different stirring

https://dx.doi.org/10.1021/acsomega.0c06328
ACS Omega 2021, 6, 8261−8270

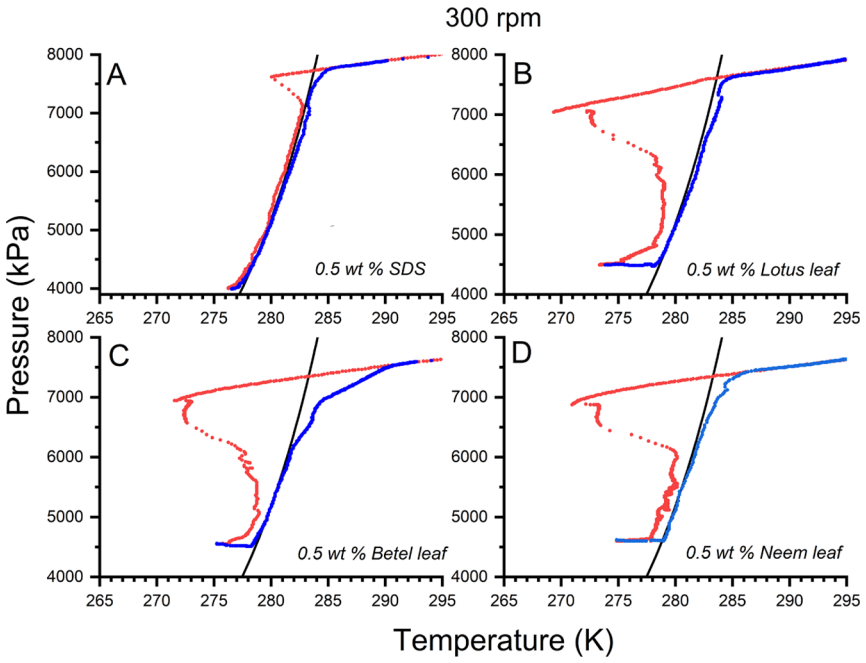

Figure 3. $p-T$ trajectories for the different biopowders performed at 300 rpm: (A) 0.5 wt % SDS, (B) 0.5 wt % lotus leaf, (C) 0.5 wt % betel leaf, and (D) 0.5 wt % neem leaf. The red dotted line indicates the cooling cycle, and the blue dotted indicates the thawing cycle. The black line is the theoretical phase boundary curve for methane hydrate computed from CSM GEM.

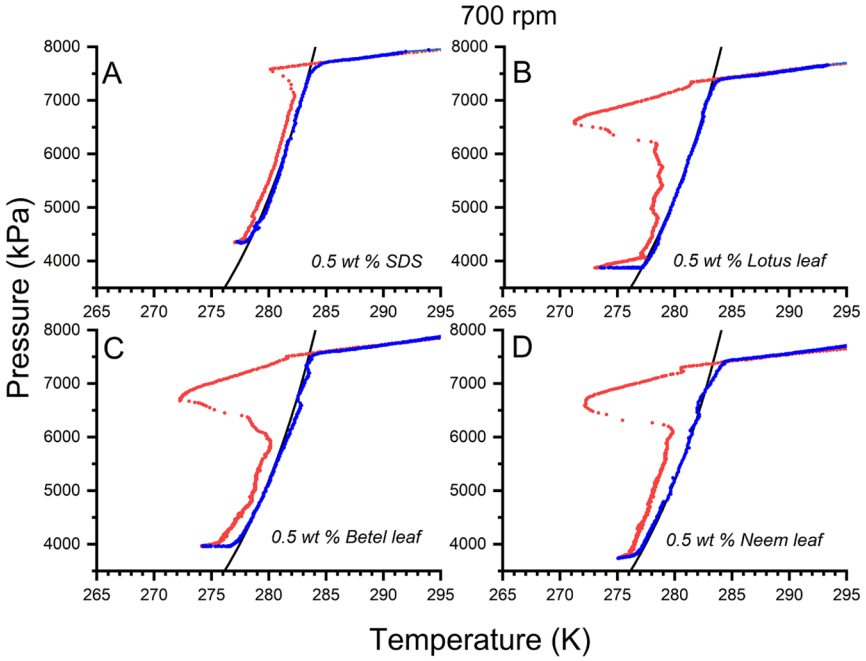

Figure 4. $p-T$ trajectories for the different biopowders performed at 700 rpm: (A) 0.5 wt % SDS, (B) 0.5 wt % lotus leaf, (C) 0.5 wt % betel leaf, and (D) 0.5 wt % neem leaf. The red dotted line indicates the cooling cycle, and the blue dotted indicates the thawing cycle. The black line is the theoretical phase boundary curve for methane hydrate computed from CSM GEM.

speeds ranging from 0 to 1000 rotations per minute (rpm). The stirrer headward is placed on the vessel and clamped tightly together with adjustable screws. Methane gas with desired pressure is filled into the reactor vessel through the inlet valve using a Teledyne ISCO syringe pump. Before introducing the gas, the reactor cell is purged with sample gas 3−4 times. The pump is disconnected after introducing the gas. The coolant circulation pipes are connected to the reactor vessel. The chiller is set to the desired experimental value to increase or decrease the reactor vessel's temperature. The stirred head with required rpm is put into action with an adjustable motor speed controller. The MH formation is inferred from the temperature spike because of the exothermic heat release during the hydrate crystal growth. The methane gas consumed in the hydrate conversion process is calculated from the observed pressure drop. Subcooling is defined as the difference between the phase equilibrium temperature at the operating pressure and the experimental formation temper-

https://dx.doi.org/10.1021/acsomega.0c06328
ACS Omega 2021, 6, 8261−8270

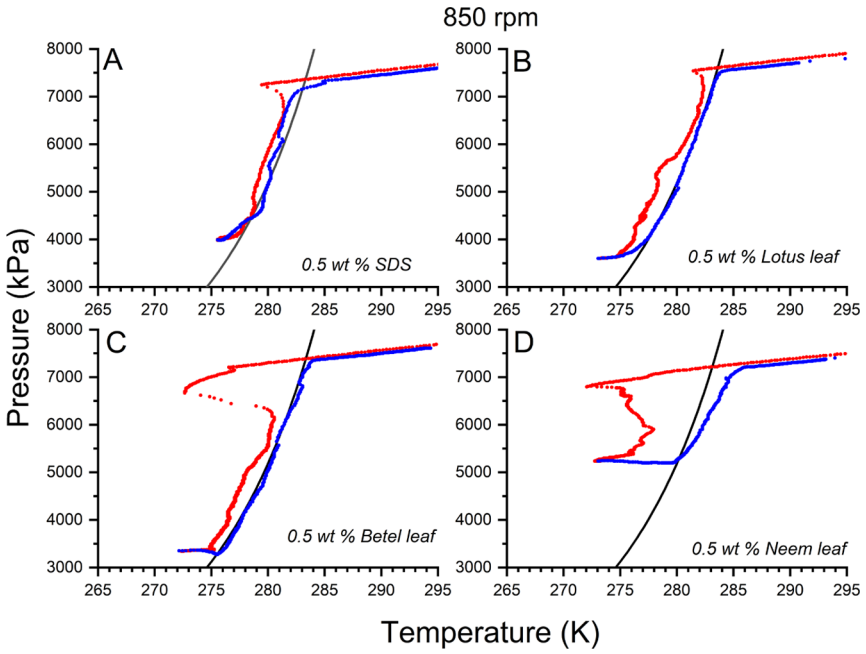

Figure 5. $p-T$ trajectories for the different bio powders performed at 850 rpm (A) 0.5 wt % SDS (B) 0.5 wt % lotus leaf (C) 0.5 wt % betel leaf (D) 0.5 wt % neem leaf. The red dotted line indicates the cooling cycle, and the blue dotted indicates the thawing cycle. The black line is the theoretical phase boundary curve for methane hydrate computed from CSM GEM.

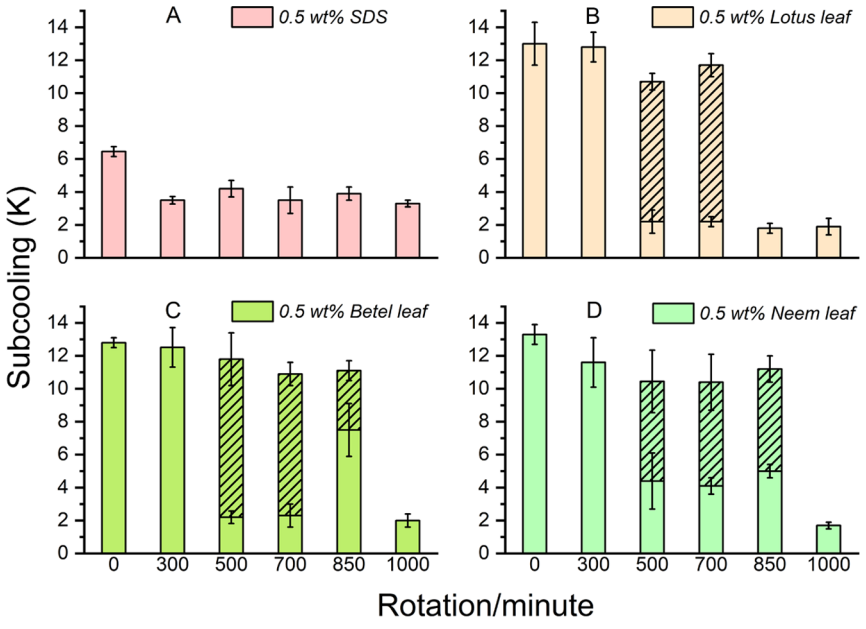

Figure 6. Comparative plot represents subcooling vs rpm. (A) 0.5 wt % SDS, (B) 0.5 wt % lotus leaf, (C) 0.5 wt % betel leaf, and (D) 0.5 wt % neem leaf. The bars with plain patterns represent primary stage nucleation, and the bars with sparse patterns represent secondary stage nucleation.

ature. The hydrate dissociation is performed at slower rates to avoid the measurable deviation from the phase boundary line. Each experiment is repeated at least three times to obtain an average value. The schematic experimental operation is shown in Figure 1. The temperature and pressure data points are recorded every 30 s. The following equation defines the molar gas concentration of methane gas in the solidified hydrate phase during an experiment at any given time t

$$\Delta nH, t = ng, 0 - ng, t = \left[\frac{P_0V}{Z_0RT_0}\right] - \left[\frac{P_tV}{Z_tRT_t}\right] \quad (1)$$

where Z is the compressibility factor, calculated using the Peng–Robinson equation of state, P is the pressure, V is the volume, T is the temperature, R is the gas constant, 0 is the initial point, and t is a point at any given time.

The volume changes during phase transformation are neglected, and the volume is constant throughout the experiment.

RESULTS AND DISCUSSION

A series of experiments are performed to understand the role of natural powders in methane hydrate formation. The primary interest is to test the extent of thermodynamic inhibition in the

https://dx.doi.org/10.1021/acsomega.0c06328
ACS Omega 2021, 6, 8261−8270

Table 1. Average Values of Measured Parameters such as Total Gas Uptake, Induction Time, Subcooling, and Yield during Hydrate Formation

rotation/minute	n_{CH4} (mol/mol H_2O)	induction time (min)	subcooling ΔT (K)	% H_2O conversion
		Sodium Dodecyl Sulfate		
0	0.078 ± 0.003[a]	21.6 ± 1	6.5 ± 0.3	49 ± 1.8
300	0.077 ± 0.003[a]	7.7 ± 0.6	3.5 ± 0.8	48.4 ± 2.1
500	0.08 ± 0.004[a]	9 ± 1.3	4.2 ± 0.5	53.2 ± 1.6
700	0.073 ± 0.003[a]	7.3 ± 1.7	3.5 ± 0.8	45.9 ± 2.1
850	0.073 ± 0.002[a]	8.5 ± 1	3.9 ± 0.4	45.8 ± 1.5
1000	0.067 ± 0.002[a]	7.3 ± 0.57	3.3 ± 0.2	42.1 ± 1.09
		Lotus Leaf Extract		
0	0.119 ± 0.005[a]	194.2 ± 45.6	13 ± 1.3	75.1 ± 3.2
300	0.064 ± 0.004[a]	33.6 ± 3.3	12.8 ± 0.9	40.1 ± 2.7
500	0.009 ± 0.003[a]	4.7 ± 1.8	2.2 ± 0.7	5.6 ± 1.6
	0.068 ± 0.001[b]	30.2 ± 3.9	8.5 ± 0.5	42.5 ± 1.8
700	0.009 ± 0.001[a]	4.6 ± 0.7	2.2 ± 0.3	5.9 ± 1.5
	0.068 ± 0.001[b]	27.2 ± 1	9.5 ± 0.7	42.9 ± 1.6
850	0.088 ± 0.002[a]	4 ± 0.5	1.8 ± 0.3	55.3 ± 1.4
1000	0.076 ± 0.004[a]	4.4 ± 1.1	1.9 ± 0.5	47.5 ± 2.2
		Betel Leaf Extract		
0	0.117 ± 0.012[a]	222.7 ± 92.9	12.8 ± 0.3	73.9 ± 7.6
300	0.063 ± 0.004[a]	33 ± 4.7	12.5 ± 1.2	39.7 ± 2.6
500	0.007 ± 0.003[a]	4.4 ± 0.7	2.2 ± 0.4	4.4 ± 2.1
	0.064 ± 0.004[b]	28.5 ± 2	9.6 ± 1.6	40.1 ± 2.5
700	0.010 ± 0.002[a]	4.8 ± 1.4	2.3 ± 0.7	6.29 ± 1.1
	0.068 ± 0.002[b]	26.2 ± 3.3	8.6 ± 0.7	42.7 ± 0.9
850	0.007 ± 0.001[a]	17 ± 3.9	7.5 ± 1.6	2.9 ± 2.6
	0.079 ± 0.004[b]	15 ±2.5	3.6 ± 0.6	49.7 ± 2.8
1000	0.08 ± 0.001[a]	4.4 ±1.1	2 ± 0.4	50.8 ± 1.8
		Neem Leaf Extract		
0	0.1 ± 0.001[a]	391.7 ± 206.8	13.3 ± 0.6	62.8 ± 0.3
300	0.057 ± 0.01[a]	32.5 ± 6.6	11.6 ± 1.5	35.8 ± 6.5
500	0.003 ± 0.001[a]	10.3 ± 4.5	4.4 ± 1.7	1.8 ± 1.3
	0.041 ± 0.009[b]	20.5 ± 3.7	6 ± 1.9	25.6 ± 5.7
700	0.008 ± 0.001[a]	8.3 ± 0.8	4.1 ± 0.5	4.8 ± 1
	0.066 ± 0.008[b]	19.2 ± 3.3	6.3 ± 1.7	41.3 ± 5.1
850	0.002 ± 0.001[a]	11.5 ± 1.4	5 ± 0.4	1.13 ± 1.2
	0.034 ± 0.009[b]	20.5 ± 3.5	6.2 ± 0.8	21.5 ± 5.8
1000	0.05 ± 0.006[a]	3.5 ± 0.4	1.7 ± 0.2	32.6 ± 3.9

[a]Measured parameters during primary nucleation. [b]Measured parameters during secondary nucleation.

H_2O-CH_4 system by adding the water-soluble extracts from the biopowders. Experiments were performed at different stirring speeds, i.e., 0, 300, 500, 700, 850, and 1000 rpm. The aqueous solution is prepared by adding 0.5 wt % dried biopowders to water and mixing them thoroughly at ambient temperature. The required amount of aqueous solution for hydrate synthesis was decanted and filtered. All of the experiments' initial point was at methane pressure ∼7.5 MPa and ambient (298 K) temperature.

In the first step, all three samples, *N. nucifera* (Indian lotus), *P. betel* (betel), and *A. indica* (neem), were tested for hydrate formation without any agitation, i.e., 0 rpm. Figure 2 shows the three natural samples' temperature and pressure trajectory (B, lotus leaf; C, betel leaf; D, neem leaf). The hydrate formation by SDS (a well-known kinetic hydrate promoter) is shown in segment A. Without any additive (pure water), the system where no hydrate nucleation is triggered is shown as a test (reference) experiment in segment A. The biopowders act as efficient THIs. Once the nucleation triggers, they act as kinetic hydrate promoters. Since sodium dodecyl sulfate is an excellent kinetic hydrate promoter in both stirred and nonstirred geometries, the obtained results are compared with the SDS system. The red dots represent the formation cycle, and the blue dots represent the dissociation pattern. The black line represents the phase equilibrium curve for the MH (sI) hydrate generated using CSM GEM software.[1] It is evident from Figure 2 that MH formed by the biopowders requires higher subcooling ∼ at 12−13 K from actual phase equilibrium temperature.

In contrast, the aqueous system with SDS requires ∼ 6 K subcooling. The subcooling is measured as the difference between the phase equilibrium temperature and the hydrate nucleation temperature. Upon crossing the maximum subcooling, the hydrate growth triggers, indicated by a temperature rise (exothermic heat) and an abrupt reduction in the pressure. The gas consumed or the amount of hydrate conversion in the cooling process is calculated using eq 1. The hydrate dissociation represents the addition of biopowders that favors the sI structure. The dissociation pattern variation from the actual phase equilibrium curve could be due to a faster heating rate. The typical heating rate in the present case is 1.5 K/h. Placement of the thermal probe in the hydrate crystallizer and

https://dx.doi.org/10.1021/acsomega.0c06328
ACS Omega 2021, 6, 8261−8270

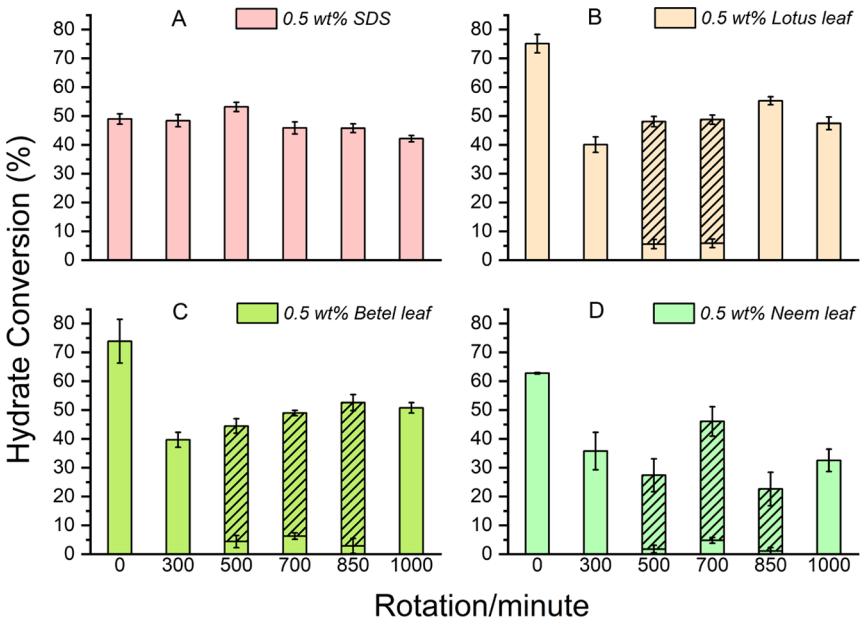

Figure 7. Comparative plot represents hydrate conversion v/s rpm. (A) 0.5 wt % SDS, (B) 0.5 wt % lotus leaf, (C) 0.5 wt % betel leaf, and (D) 0.5 wt % neem leaf. The bars with plain patterns represent primary stage nucleation, and the bars with sparse patterns represent secondary stage nucleation.

the nature of some unknown constitutes in the biopowders could also potentially contribute to the apparent deviations. However, higher subcooling, often required for hydrate nucleation in the presence of bioextracts, is a useful observation in preventing hydrate formation.

Further, the experiments were conducted with a magnetic agitation to probe the hydrate formation. It is well known that such agitation improves the hydrate formation ability. The laboratory-scale investigations in continuously stirred or rocking cells provide valuable information about the process.[47,52,53] They thus can be adopted to understand the behavior in a typical flow loop.

As the beginning step, the experiments are performed at a lower speed, i.e., 300 rpm. Figure 3 represents the temperature and pressure profiles in cooling and warming cycles. A careful comparison between the nonstirred and stirred (300 rpm) geometries resulted in the following: (a) the required subcooling for SDS has decreased by about 2 K, whereas it remained more or less similar in bioextract additives. (b) Notably, the hysteresis width between the freezing and thawing cycles, particularly for bioadditives, decreased, indicating that the hydrate growth is distributed in smaller clusters. During the continuous stirring process, the gas molecules would interact with new water molecules, and the interaction could trigger poly nucleus sites for the hydrates.[1] Further, the process was investigated by changing the rotation speed to higher rpm, i.e., 500 and 700. Figure 4 shows the hydrate formation and dissociation pattern at 700 rpm. The pressure and temperature profiles in 500 and 700 rpm followed the same as those in 300 rpm. The required subcooling is preserved at ∼ 10−12 K for all of the three biopowders. However, hydrate formation is observed to be a two-stage nucleation process. The primary nucleation point is marked around temperatures 281.2 ± 0.05, 281.1 ± 0.14, and 279.8 ± 1.5 K for the lotus, betel, and neem leaves. The secondary stage nucleation where the hydrate growth is maximum is around 272.2 ± 0.7, 271.9 ± 0.6, and 273.5 ± 1.3 K temperatures. The stirring effect on SDS additives in 500 and 700 rpm is the same as that in the 300 rpm, where the required subcooling is around 3.85 ± 0.4 K. The SDS hydrates grow in the single-stage process once the necessary subcooling prevails. Several studies have reported that methane hydrate formation could occur in a two-stage phenomenon. Jacobson et al. performed a set of molecular simulation studies on the nucleation and growth of a hydrophobic guest's clathrates, which have clathrate-forming properties similar to methane and carbon dioxide. The study reports the first step, blob formation, which are long-lived aggregates of guests separated by water molecules. The clathrate cages repeatedly nucleate and dissolve until a cluster of cages reaches the critical size, which prompts space filling of face-sharing clathrate cages. The clathrate formed in this process is amorphous and is in a metastable window growing into crystalline clathrate. Ripening of the amorphous phase produces nanocrystals of the stable sI clathrates.[54] Vatamanu et al. also performed molecular dynamic simulations on methane hydrate growth and nucleations. The study exposes the methane hydrate nucleation is characterized in the two-stage process. The conditions examined show the nucleation does not appear to start with the immediate formation of small crystals but initially develops some disordered solid containing a mixture of symmetric and irregular water cages. This primary nucleated structure subsequently is shown to anneal to more regular crystalline structures.[55−57]

The hydrate growth percentage from the primary nucleation to that of secondary nucleation is near ∼6%. This phenomenon is ascribed due to blobs' formation, which are long-lived aggregates of guests separated by water molecules. The clathrate formed in this stage is amorphous and in a metastable window, leading to the crystalline hydrate phase formation.[54] The time for the blobs or the polynuclei to be in the metastable phase (between the primary and secondary nucleation stages) is about 24 ± 2, 22.7 ± 1.9, and 10.6 ± 0.4 min for the lotus, betel, and neem samples, respectively.

https://dx.doi.org/10.1021/acsomega.0c06328
ACS Omega 2021, 6, 8261−8270

Further experiments were carried out by increasing the rotation speed to 850 and 1000 rpm. Figure 5 shows the methane hydrate formation at a rotation speed of 850 rpm. Interestingly, the observations show that nucleation in the lotus leaf sample is triggered by increasing the rotation speed to 850 and 1000 rpm. Hydrate formation around the primary nucleation point (281.42 ± 0.4 and 281.8 ± 0.3) and the hydrate growth is prompt. The two-step nucleation is not observed, and the amount of subcooling required is only 2 K. However, in the case of betel and neem leaf samples, the thermodynamic inhibition is shown up to 850 rpm, and further increasing the rotation speed to 1000, the hydrate nucleation is triggered around 281.35 ± 0.03 and 281.6 ± 0.1 K and the subcooling is lowered to 2 K. It is evident that with increasing the rotation speed the hydrate particles tend to grow at the primary nucleation point. Recent studies report that water depth and gas production rate are triggering the hydrate occurrence in the pipeline. The hydrate layer growth rate is maximum when the gas flow is low, making a path for the water droplets to interact with the gas and constructively develop the hydrate around the walls of the pipelines (lower rpm), and also when the depth of water increases, the hydrate growth is faster due to the lower temperatures (supercooling).

Similarly, at higher gas flow rates, hydrates formed from the water droplets are often transported by gas due to high gas velocity.[58] With an increase in the stirring speed, the particles' velocity in the reactor increases, and the formed seed crystals would spread across the bulk phase and transform the hydrate growth rapidly and efficiently.[1] Skovborg et al. studied the methane and ethane hydrate formation at different rpm's (200, 250, 300, and 380). The study reported that an increase in the stirring rate reduces the induction time. Agitation enhances interfacial mass transport, thereby quickening the hydrate growth.[59] Parent et al. also stated stirring would flatten the temperature and composition gradients in the bulk phase, advance heat and mass transmission efficiency, and therefore give faster formation.[60] Svandal et al. and others also proposed that the induction time of hydrate formation becomes shorter at higher stirring rates.[61,62] From the earlier studies, it is clear that higher rotations influence the hydrate formation conditions. The MH formation with the natural biopowders has shown higher subcooling when compared with SDS. With increasing rpm, the lotus leaf showed higher subcooling up to 700 rpm. After crossing the threshold rotation speed, the hydrate nucleated at the primary nucleation point. As discussed, higher stirring rates would affect the temperature and composition gradients, advance heat and mass transmission efficiency, and therefore provide faster growth.[59,60] For the lotus leaf, the threshold rpm is up to 700 rpm when the effective subcooling prevails and thereafter the sample extracts do not show thermodynamic inhibition due to higher rotations. Similarly, the same is true with the betel and neem leaves where the threshold rotations are around 850 rpm. After crossing the threshold rpm, the thermodynamic inhibition property is lowered.

The comparative plot of subcooling required with the biopowders is shown in Figure 6. The hydrates formed with SDS require lesser subcooling and are relatively constant with increasing rotation speed. The surfactant particles homogeneously promote hydrate growth and do not show deviation in required subcooling. Somehow the biopowders show the highest inhibition on MH formation. With increasing rotation speed, the hydrate formation temperature is influenced. The biopowder extracts act as good inhibitors until their respective threshold agitation limits. It is evident that the biopowders are suitable and work effectively as THIs. They are less appropriate to serve as KHIs since the hydrate growth is rapid, and 90% of the hydrate growth is less than 90 min. The induction time is within 30 min for the hydrate to trigger; detailed data of the experimental runs are shown in Table 1. All of the experiments are repeated at least three times to check the repeatability and consistency of the data. The sequential order of the biopowders from high to low, depending on their thermodynamic inhibition, gas uptake, and hydrate conversion, is NL > BL > LL > SDS.

Figure 7 represents hydrate conversion at different rotation speeds. With no agitation in the system, water transformation to the hydrate phase is almost 70%, where the hydrate growth is continuous upon the formation of a seed crystal. In stirring, the hydrate conversion decreased to 40−50%, where the seed particles are not allowed to grow continuously. From primary nucleation to secondary nucleation, the hydrate conversion is 6%, which is shown in the plain pattern.

The exact reason for the inhibitory function of these bioadditives is not clearly understood. It requires further detailed investigations. On the other hand, Xu et al. reported pectin as a methane hydrate inhibitor. The inhibition effect is ascribed to the oxygen atoms in carboxyl and hydroxyl groups of pectin, which forms hydrogen bonds with water molecules, which will disrupt the water structure. The hydrophilic structure enables pectin to retard crystal growth. Oxygen atoms of pectin bind to the surface of hydrate crystal through hydrogen bonds.[38] Similarly, Elechi et al. reported the inhibitory effect of a medicinal plant extract named Costaceae, which contains a wide variety of bioactive compounds like phenols and alkaloids, flavonoids, tannins, and saponins. These compounds could be responsible for assisting the hydrate formation at lower temperatures.[42] Similarly, all three bioadditives constitute several bioactive compounds. The neem leaf extracts may contain triterpenoids, alkaloids, phenolic compounds, flavonoids, carotenoids, ketones, and steroids. The most biologically active compound is azadirachtin. Phytochemistry screening of neem leaf extracts revealed the presence of tannins, saponins, flavonoids, alkaloids, glycosides, reducing sugars, and polyphenols.[63] The betel leaf named *P. betel* belongs to the Piperaceae family. Betel leaves contain reasonable amounts of vitamins, particularly nicotinic acid, ascorbic acid, and carotin. They also comprise all essential amino acids except glycine, histidine, and arginine. High concentrations of asparagines are present, while glycine and proline occur in a reasonable amount.[64] The lotus leaf possesses pharmacologic and physiologic compounds, which exhibit hepatoprotective, antioxidant, antidiarrheal, antiviral, immunomodulatory, and antiobesity effects. The leaves also contain several flavonoids and alkaloids.[65] All three classes of leaves possess several bioactive components, which mostly consist of proteins and antioxidants. Close observations indicate that these antioxidants that inhibit the reactions promoted by oxygen compounds could be responsible for hydrate nucleation to occur at lower temperatures. A detailed study is required in understanding the microlevel analysis of these components. At present, the study exposes that natural biopowders in low concentrations (0.5 wt %) can act as effective thermodynamic inhibitors for MH. These biodegradable additives are marked to be very useful and reduce traditional inhibitors in real-time applications.

https://dx.doi.org/10.1021/acsomega.0c06328
ACS Omega 2021, 6, 8261−8270

CONCLUSIONS

In summary, we investigated the methane hydrate formation behavior in an aqueous solution consisting of soluble biodegradable additives, namely, *A. indica* (neem), *P. betel* (betel), and *N. nucifera* (Indian lotus). The addition of these bioadditives in low dosages (0.5 wt %) demands higher subcooling (~10 to 12 K) for the onset of methane hydrate formation. Neem leaf powder showed the best result, and remarkably, the hydrate growth percentage is lowered by 30% compared with that of SDS. The next best outcome is elucidated by betel leaf. Lotus leaf shows functional inhibition until the rotation speed exceeds the maximum threshold limit. Thus, the addition of bioadditives significantly delays the methane hydrate formation in both stirred (up to threshold rpm) and nonstirred geometries. The required subcooling is 12−13 K from the actual-phase equilibrium curve. Conclusively, three bioadditives have been identified, which have the competency to act as potential THIs for methane hydrates.

AUTHOR INFORMATION

Corresponding Author

Pinnelli S. R. Prasad − *Academy of Scientific and Innovative Research (AcSIR), Ghaziabad 201002, India; Gas Hydrate Division, CSIR−National Geophysical Research Institute (CSIR−NGRI), Hyderabad 500007, India;* orcid.org/0000-0003-1473-5510; Phone: +91 40 2701 2710; Email: psrprasad@ngri.res.in; Fax: +91 40 2717 1564

Author

Burla Sai Kiran − *Academy of Scientific and Innovative Research (AcSIR), Ghaziabad 201002, India; Gas Hydrate Division, CSIR−National Geophysical Research Institute (CSIR−NGRI), Hyderabad 500007, India*

Complete contact information is available at: https://pubs.acs.org/10.1021/acsomega.0c06328

Notes

The authors declare no competing financial interest.

ACKNOWLEDGMENTS

The authors sincerely thank the Director of the National Geophysical Research Institute, Hyderabad, for his encouragement and permission to publish this paper (NGRI/Lib/2020/Pub-95). The authors appreciate G. Rama Rao, N. Chanikya, and T. Bhavya in conducting experiments. Partial financial support from MoES (India) and DGH-NGHP (India) is acknowledged.

REFERENCES

(1) Sloan, D.; Koh, C. A.; Koh, C. A. *Clathrate Hydrates of Natural Gases*; 3rd ed.; CRC Press, 2007.

(2) *Natural Gas Hydrates in Flow Assurance*; Sloan, D.; Koh, C.; K. Sum, A.; L. Ballard, A.; Creek, J.; Eaton, M.; Lachance, J.; McMullen, N.; Palermo, T.; Shoup, G.; Talley, L., Eds.; Gulf Professional Publishing: Boston, 2011; p iv.

(3) Makogon, Y. F. Hydrate formation in the gas-bearing beds under permafrost conditions. *Gazovaia Prom-st.* **1965**, *5*, 14−15.

(4) Englezos, P.; Lee, J. D. Gas hydrates: A cleaner source of energy and opportunity for innovative technologies. *Korean J. Chem. Eng.* **2005**, *22*, 671−681.

(5) Makogon, Y. F.; Holditch, S. A.; Makogon, T. Y. Natural gas-hydrates — A potential energy source for the 21st Century. *J. Pet. Sci. Eng.* **2007**, *56*, 14−31.

(6) Hammerschmidt, E. G. Formation of Gas Hydrates in Natural Gas Transmission Lines. *Ind. Eng. Chem.* **1934**, *26*, 851−855.

(7) Sloan, E. D. Fundamental principles and applications of natural gas hydrates. *Nature* **2003**, *426*, 353−359.

(8) Sloan, E. D. A changing hydrate paradigm—from apprehension to avoidance to risk management. *Fluid Phase Equilib.* **2005**, *228−229*, 67−74.

(9) Koh, C. A.; Westacott, R. E.; Zhang, W.; Hirachand, K.; Creek, J. L.; Soper, A. K. Mechanisms of gas hydrate formation and inhibition. *Fluid Phase Equilib.* **2002**, *194−197*, 143−151.

(10) Sa, J.-H.; Kwak, G. H.; Han, K.; Ahn, D.; Cho, S. J.; Lee, J. D.; Lee, K. H. Inhibition of methane and natural gas hydrate formation by altering the structure of water with amino acids. *Sci. Rep.* **2016**, *6*, No. 31582.

(11) Prasad, P. S. R. Methane Hydrate Formation and Dissociation in the Presence of Hollow Silica. *J. Chem. Eng. Data* **2015**, *60*, 304−310.

(12) Kiran, B. S.; Prasad, P. S. R. Storage of Methane Gas in the Form of Clathrates in the Presence of Natural Bioadditives. *ACS Omega* **2018**, *3*, 18984−18989.

(13) Prasad, P. S. R.; Sai Kiran, B. Clathrate Hydrates of Greenhouse Gases in the Presence of Natural Amino Acids: Storage, Transportation and Separation Applications. *Sci. Rep.* **2018**, *8*, No. 8560.

(14) Karamoddin, M.; Varaminian, F. Water desalination using R141b gas hydrate formation. *Desalin. Water Treat.* **2014**, *52*, 2450−2456.

(15) Fakharian, H.; Ganji, H.; Naderifar, A. Desalination of high salinity produced water using natural gas hydrate. *J. Taiwan Inst. Chem. Eng.* **2017**, *72*, 157−162.

(16) Adisasmito, S.; Parubak, E. *Ethylene Glycol Injection for Hydrate Formation Prevention in Deepwater Gas Pipelines*, MATEC Web of Conferences; EDP Sciences, 2019; p 02003.

(17) Qureshi, M. F.; Atilhan, M.; Altamash, T.; Tariq, M.; Khraisheh, M.; Aparicio, S.; Tohidi, B. Gas Hydrate Prevention and Flow Assurance by Using Mixtures of Ionic Liquids and Synergent Compounds: Combined Kinetics and Thermodynamic Approach. *Energy Fuels* **2016**, *30*, 3541−3548.

(18) Ding, L.; Shi, B.; Lv, X.; Liu, Y.; Wu, H.; Wang, W.; Gong, J. Hydrate Formation and Plugging Mechanisms in Different Gas−Liquid Flow Patterns. *Ind. Eng. Chem. Res.* **2017**, *56*, 4173−4184.

(19) Khan, M. S.; Lal, B.; Partoon, B.; Keong, L. K.; Bustam, A. B.; Mellon, N. B. Experimental Evaluation of a Novel Thermodynamic Inhibitor for CH4 and CO2 Hydrates. *Procedia Eng.* **2016**, *148*, 932−940.

(20) Tariq, M.; Rooney, D.; Othman, E.; Aparicio, S.; Atilhan, M.; Khraisheh, M. Gas Hydrate Inhibition: A Review of the Role of Ionic Liquids. *Ind. Eng. Chem. Res.* **2014**, *53*, 17855−17868.

(21) Semenov, A. P.; Stoporev, A. S.; Mendgaziev, R. I.; Gushchin, P. A.; Khlebnikov, V. N.; Yakushev, V. S.; Istomin, V. A.; Sergeeva, D. V.; Vinokurov, V. A. Synergistic effect of salts and methanol in thermodynamic inhibition of sII gas hydrates. *J. Chem. Thermodyn.* **2019**, *137*, 119−130.

(22) Semenov, A. P.; Mendgaziev, R. I.; Stoporev, A. S.; Gushchina, Y. F.; Anikushin, B. M.; Gushchin, P. A.; Khlebnikov, V. N. Synergism of Methanol and Magnesium Chloride for Thermodynamic Inhibition of Methane Hydrate. *Chem. Technol. Fuels Oils* **2019**, *54*, 738−742.

(23) Qasim, A.; Khan, M. S.; Lal, B.; Ismail, M. C.; Rostani, K. Quaternary ammonium salts as thermodynamic hydrate inhibitors in the presence and absence of monoethylene glycol for methane hydrates. *Fuel* **2020**, *259*, No. 116219.

(24) Adisasmito, S.; Parubak, E. Ethylene glycol injection for hydrate formation prevention in deepwater gas pipelines. *MATEC Web Conf.* **2019**, *268*, No. 02003.

(25) Cha, M.; Shin, K.; Kim, J.; Chang, D.; Seo, Y.; Lee, H.; Kang, S. P. Thermodynamic and kinetic hydrate inhibition performance of aqueous ethylene glycol solutions for natural gas. *Chem. Eng. Sci.* **2013**, *99*, 184−190.

(26) Altamash, T.; Aparicio, S.; Atilhan, M. An experimental study on doubly salt effect for methane hydrate inhibition. *J. Nat. Gas Sci. Eng.* **2019**, *72*, No. 103015.
(27) Cheng, L. W.; Liao, K.; Li, Z.; Cui, J. L.; Liu, B.; Li, F. G.; Chen, G. J.; Sun, C. Y. The invalidation mechanism of kinetic hydrate inhibitors under high subcooling conditions. *Chem. Eng. Sci.* **2019**, *207*, 305−316.
(28) Cheng, L.; Wang, L.; Li, Z.; Liu, B.; Chen, G. Inhibition Effect of Kinetic Hydrate Inhibitors on the Growth of Methane Hydrate in Gas−Liquid Phase Separation State. *Energies* **2019**, *12*, No. 4482.
(29) Sharifi, H.; Walker, V. K.; Ripmeester, J.; Englezos, P. Insights into the Behavior of Biological Clathrate Hydrate Inhibitors in Aqueous Saline Solutions. *Cryst. Growth Des.* **2014**, *14*, 2923−2930.
(30) Mady, M. F.; Kelland, M. A. N,N-Dimethylhydrazidoacrylamides. Part 2: High-Cloud-Point Kinetic Hydrate Inhibitor Copolymers with N- Vinylcaprolactam and Effect of pH on Performance. *Energy Fuels* **2015**, *29*, 678−685.
(31) Zhang, Q.; Kelland, M. A.; Ajiro, H. Polyvinylsulfonamides as Kinetic Hydrate Inhibitors. *Energy Fuels* **2020**, *34*, 2230−2237.
(32) Zhang, Y. D.; Shen, X. D.; Maeda, N. Synergism of Ethers on the Kinetic Inhibition Performance of Poly(N-vinyl pyrrolidone) on Methane Hydrate in a Pilot-Scale Flow Loop. *Energy Fuels* **2020**, *34*, 2790−2799.
(33) Ree, L. H. S.; Kelland, M. A. Investigation of Solvent Synergists for Improved Kinetic Hydrate Inhibitor Performance of Poly(N-isopropyl methacrylamide). *Energy Fuels* **2019**, *33*, 8231−8240.
(34) Perrin, A.; Musa, O. M.; Steed, J. W. The chemistry of low dosage clathrate hydrate inhibitors. *Chem. Soc. Rev.* **2013**, *42*, 1996−2015.
(35) Bui, T.; Sicard, F.; Monteiro, D.; Lan, Q.; Ceglio, M.; Burress, C.; Striolo, A. Antiagglomerants Affect Gas Hydrate Growth. *J. Phys. Chem. Lett.* **2018**, *9*, 3491−3496.
(36) Lv, Y. N.; Guan, Y. T.; Guo, S. D.; Ma, Q. L.; Gong, J.; Chen, G. J.; Sun, C. Y.; Guo, K.; Yang, L. Y.; Shi, B. H.; Qin, W.; Qiao, Y. B. Effects of Combined Sorbitan Monolaurate Anti-Agglomerants on Viscosity of Water-in-Oil Emulsion and Natural Gas Hydrate Slurry. *Energies* **2017**, *10*, No. 1105.
(37) Kelland, M. A. History of the development of low dosage hydrate inhibitors. *Energy Fuels* **2006**, *20*, 825−847.
(38) Xu, S.; Fan, S.; Fang, S.; Lang, X.; Wang, Y.; Chen, J. Pectin as an Extraordinary Natural Kinetic Hydrate Inhibitor. *Sci. Rep.* **2016**, *6*, No. 23220.
(39) Tian, L. Q.; Wu, G. Z. Cyclodextrins as promoter or inhibitor for methane hydrate formation? *Fuel* **2020**, *264*, No. 116828.
(40) Mollashahi Sanatgar, S.; Peyvandi, K. New edible additives as green inhibitors for preventing methane hydrate formation. *J. Environ. Chem. Eng.* **2019**, *7*, No. 103172.
(41) Efiong, O. O.; Atubokiki, A. J.; Sunday, I. S.; Urunwo, E. V.; Olabisi, O. T. Use of Locally Formulated Inhibitor from Agro Waste for Gas Hydrate Inhibition in a Mini Flow Loop. *Int. J. Sci. Eng. Invest.* **2018**, *7*, 104−112.
(42) Elechi, V. U.; Ikiensikimama, S. S.; Akaranta, O.; Ajienka, J. A.; Okon, O. E. , Investigation of Plant Family Costaceae Extract as Gas Hydrate Inhibitor in a Simulated Offshore Environment. *Int. J. Sci. Eng. Invest.* **2019**, *8*, 92−102.
(43) Tang, C. P.; Liang, D. Q. Inhibitory effects of novel green inhibitors on gas hydrate formation. *Chin. J. Chem. Eng.* **2019**, *27*, 2107−2117.
(44) Prasad, P. S. R.; Kiran, B. S. Are the amino acids thermodynamic inhibitors or kinetic promoters for carbon dioxide hydrates? *J. Nat. Gas Sci. Eng.* **2018**, *52*, 461−466.
(45) Lee, D.; Go, W.; Ko, G.; Seo, Y. Inhibition synergism of glycine (an amino acid) and [BMIM][BF4] (an ionic liquid) on the growth of CH4 hydrate. *Chem. Eng. J.* **2020**, *393*, No. 124466.
(46) da Silva Ramos, A.; Pires, J. P.; Medina Ketzer, J. M.; Espíndola de Araújo, G.; Lourega, R. V. Synthesis of new CO2 hydrate inhibitors. *J. Nat. Gas Sci. Eng.* **2020**, *75*, No. 103166.
(47) Altamash, T.; Qureshi, M. F.; Aparicio, S.; Aminnaji, M.; Tohidi, B.; Atilhan, M. Gas hydrates inhibition via combined biomolecules and synergistic materials at wide process conditions. *J. Nat. Gas Sci. Eng.* **2017**, *46*, 873−883.
(48) Farhadian, A.; Varfolomeev, M. A.; Shaabani, A.; Nasiri, S.; Vakhitov, I.; Zaripova, Y. F.; Yarkovoi, V. V.; Sukhov, A. V. Sulfonated chitosan as green and high cloud point kinetic methane hydrate and corrosion inhibitor: Experimental and theoretical studies. *Carbohydr. Polym.* **2020**, *236*, No. 116035.
(49) Farhadian, A.; Varfolomeev, M. A.; Shaabani, A.; Zaripova, Y. F.; Yarkovoi, V. V.; Khayarov, K. R. Inhibition Performance of Chitosan-graft-Polyacrylamide as an Environmentally Friendly and High-Cloud-Point Inhibitor of Nucleation and Growth of Methane Hydrate. *Cryst. Growth Des.* **2020**, *20*, 1771−1778.
(50) Vysniauskas, A.; Bishnoi, P. R. A kinetic study of methane hydrate formation. *Chem. Eng. Sci.* **1983**, *38*, 1061−1072.
(51) Al-Adel, S.; Dick, J. A. G.; El-Ghafari, R.; Servio, P. The effect of biological and polymeric inhibitors on methane gas hydrate growth kinetics. *Fluid Phase Equilib.* **2008**, *267*, 92−98.
(52) Daraboina, N.; Linga, P.; Ripmeester, J.; Walker, V. K.; Englezos, P. Natural Gas Hydrate Formation and Decomposition in the Presence of Kinetic Inhibitors. 2. Stirred Reactor Experiments. *Energy Fuels* **2011**, *25*, 4384−4391.
(53) Sa, J.-H.; Melchuna, A.; Zhang, X.; Morales, R.; Cameirao, A.; Herri, J.-M.; Sum, A. K. Rock-Flow Cell: An Innovative Benchtop Testing Tool for Flow Assurance Studies. *Ind. Eng. Chem. Res.* **2019**, *58*, 8544−8552.
(54) Jacobson, L. C.; Hujo, W.; Molinero, V. Amorphous precursors in the nucleation of clathrate hydrates. *J. Am. Chem. Soc.* **2010**, *132*, 11806−11.
(55) Vatamanu, J.; Kusalik, P. G. Observation of two-step nucleation in methane hydrates. *Phys. Chem. Chem. Phys.* **2010**, *12*, 15065−72.
(56) Cacciuto, A.; Frenkel, D. Stresses inside critical nuclei. *J. Phys. Chem. B* **2005**, *109*, 6587−94.
(57) Shiau, L.-D.; Lu, Y. F. Modeling solute clustering in the diffusion layer around a growing crystal. *J. Chem. Phys.* **2009**, *130*, No. 094105.
(58) Zhao, Y.; Wang, Z.; Zhang, J.; Wang, X.; Sun, B. In *Flow Assurance During Deepwater Gas Well Testing: When and Where Hydrate Blockage Would Occur*, SPE Annual Technical Conference and Exhibition, 2016.
(59) Skovborg, P.; Ng, H. J.; Rasmussen, P.; Mohn, U. Measurement of Induction Times for the Formation of Methane and Ethane Gas Hydrates. *Chem. Eng. Sci.* **1993**, *48*, 445−453.
(60) Parent, J. S.; Bishnoi, P. R. Investigations into the nucleation behaviour of methane gas hydrates. *Chem. Eng. Commun.* **1996**, *144*, 51−64.
(61) Svandal, A.; Kvamme, B.; Granasy, L.; Pusztai, T.; Buanes, T.; Hove, J. The phase-field theory applied to CO2 and CH4 hydrate. *J. Cryst. Growth* **2006**, *287*, 486−490.
(62) Ke, W.; Svartaas, T. M. In *Effects of Stirring and Cooling on Methane Hydrate Formation in a High-Pressure Isochoric Cell*, Proceedings of the 7th International Conference on Gas Hydrates; Edinburgh, Scotland, United Kingdom, 2011.
(63) Eid, A.; Jaradat, N.; Elmarzugi, N. J. P. M.; Journal, P. A Review of chemical constituents and traditional usage of Neem plant (*Azadirachta Indica*). *Palestinian Med. Pharm. J.* **2017**, *2*, 75−81.
(64) Sengupta, R.; Banik, J. K. Research, A review on betel leaf (pan). *Int. J. Pharm. Sci. Res.* **2013**, *4*, 4519.
(65) Huang, C. F.; Chen, Y. W.; Yang, C. Y.; Lin, H. Y.; Way, T. D.; Chiang, W.; Liu, S. H. Extract of lotus leaf (*Nelumbo nucifera*) and its active constituent catechin with insulin secretagogue activity. *J. Agric. Food Chem.* **2011**, *59*, 1087−94.

https://dx.doi.org/10.1021/acsomega.0c06328
ACS Omega 2021, 6, 8261−8270